Oblique fluorescence in a MARS scanner with a CdTe-Medipix3RX

2016 JINST 11 C12063

(http://iopscience.iop.org/1748-0221/11/12/C12063)

Jinst

Published by IOP Publishing for Sissa Medialab

Received: *September 29, 2016*
Accepted: *December 8, 2016*
Published: *December 22, 2016*

18th International Workshop on Radiation Imaging Detectors
3–7 July 2016,
Barcelona, Spain

Oblique fluorescence in a MARS scanner with a CdTe-Medipix3RX

L. Vanden Broeke,[a,1] **A. Atharifard,**[b] **B.P. Goulter,**[c] **J.L. Healy,**[d] **M. Ramyar,**[b] **R.K. Panta,**[b,c] **M. Anjomrouz,**[b] **M. Shamshad,**[b] **A. Largeau,**[e] **K. Mueller,**[f] **M.F. Walsh,**[c] **R. Aamir,**[b,c] **D.J. Smithies,**[c] **R. Doesburg,**[c] **K. Rajendran,**[b] **N.J.A. de Ruiter,**[b,c,g] **D. Knight,**[b] **A. Chernoglazov,**[c,g] **H. Mandalika,**[g] **C.J. Bateman,**[a,b,c] **S.T. Bell,**[c,h] **A.P.H. Butler**[a,b,c,h] **and P.H. Butler**[a,c,h]

[a] *Department of Physics and Astronomy, University of Canterbury, Private Bag 4800, Christchurch 8140, New Zealand*
[b] *Department of Radiology, University of Otago, Christchurch, 2 Riccarton Ave, Christchurch 8140, New Zealand*
[c] *MARS Bioimaging Ltd, 29a Clyde Rd, Christchurch, New Zealand*
[d] *Department of Biology, University of Canterbury, Private Bag 4800, Christchurch 8140, New Zealand*
[e] *Télécom Physique Strasbourg, Université de Strasbourg, Pôle API, 300 Bd Sébastien Brant, 67400 Illkirch-Graffenstaden, France*
[f] *Institut für Medizintechnik, University of Lübeck, Ratzeburger Allee 160, 23562 Lübeck, Germany*
[g] *HIT lab NZ, University of Canterbury, NZi3 Building 69 Creyke Rd, Ilam, Christchurch 8041, New Zealand*
[h] *European Organization for Nuclear Research (CERN), CH-1211 Geneva 23, Switzerland*

E-mail: lieza.vandenbroeke@pg.canterbury.ac.nz

Abstract: The latest version of the MARS small bore scanner makes use of the Medipix3RX ASIC, bonded to a CdTe or CZT semi-conductor layer, to count x-ray photons and create a spectroscopic CT data set. The MARS imaging chain uses the energy-resolved 2D transmission images to construct quantitative 3D spectral and material images. To improve the spectral performance of the imaging system it is important that the energy response of the detector is well calibrated. A common methodology for energy calibration is to use x-ray fluorescence (XRF), due to its effective

[1] Corresponding author.

doi:10.1088/1748-0221/11/12/C12063

monochromatic nature. Oblique (off-axis) XRF can be measured in situ in the MARS small bore scanner. A monoatomic foil is placed in front of the x-ray source and off-axis XRF is measured. A key issue is identifying near optimal measurement positions that maximize the XRF signal while minimizing transmitted and scattered x-rays from the primary beam.

This work shows the development of a theoretical model that is able to identify where in the detector plane XRF is maximum. We present: (1) a theoretical model that calculates the XRF photon distribution across the detector plane produced from illuminated foils attached to the scanner's filter bar; (2) preliminary experimental measurements of the XRF distribution outside of the main beam taken with a CdTe-Medipix3RX detector; and (3) a comparison between the model and experiment. The main motivation behind creating this model is to identify the region in the detector plane outside of the main beam where XRF is at a maximum. This provides the optimum detector location for measuring a monochromatic XRF source with minimal polychromatic contamination for its use in per-pixel energy calibration of Medipix3RX detectors in MARS scanners.

KEYWORDS: Computerized Tomography (CT) and Computed Radiography (CR); Solid state detectors; X-ray detectors

2016 JINST 11 C12063

Contents

1 Introduction **1**

2 Experimental setup **2**

3 Oblique fluorescence model **2**
- 3.1 Narrow beam foil illumination 3
- 3.2 Complete foil illumination 4
- 3.3 Molybdenum foil example 4

4 Preliminary experiments **5**
- 4.1 Methods 5
- 4.2 Results 5

5 Discussion **6**

6 Conclusion **7**

1 Introduction

The Medipix All Resolution System (MARS) is a spectral CT scanner that uses the Medipix3RX family of photon counting x-ray detectors (PCXDs). This paper introduces a methodology for measuring x-ray fluorescence (XRF) produced from illuminated metallic foils placed inside MARS scanners. In the proposed approach, the metallic foils are positioned on the front of the extrinsic filtration that is located between the x-ray source and the source collimators. When the main x-ray beam is narrowed with the collimators, wide angle (oblique) XRF reaches the detector plane outside of the main beam. As a result, this technique enables the monochromatic XRF beam produced from the metallic foil to be used for energy calibration of the scanner's PCXD with minimal contamination by the polychromatic x-rays from the main beam.

The primary advantage of using PCXDs in spectral CT is their energy discrimination capabilities. PCXDs have multiple counters per pixel. Each counter measures a different energy window. Together, the different energy windows let you identify numerous targeted materials simultaneously [1, 2]. The number of energy windows per detector pixel in PCXDs varies from 2 to 8, depending on specific detector designs [3]. MARS systems typically use CdTe or CZT Medipix3RX detectors, which have 8 counters per pixel. In order to use such detectors for material identification effectively, the energy response of each counter (in every detector pixel) needs to be calibrated. Other commonly known advantages of using PCXDs in spectral CT include a significantly higher contrast to noise ratio (CNR) [4]; a reduction of radiation dose [4]; and higher sensitivity to low-energy x-rays compared to charge-integrating detectors [5].

Calibrating the energy response of PCXDs can be achieved using various methods. Typically these are based on measurements of monochromatic x-rays which are generated from either metallic

2016 JINST 11 C12063

foil XRF [6–8], synchrotron radiation [9], or radioactive sources [10]. However it is also possible to calibrate using the kVp energy of a polychromatic x-ray spectrum [11]. Each of these four calibration sources present their own limitations and difficulties in calibrating PCXDs in spectral CT setups. XRF can be contaminated by polychromatic x-rays from the x-ray source that is used to induce excitation in the foil; synchrotrons require a large physical space for their setup and have significant cost; long measurement times are needed for radioactive sources; and accuracy of the kVp methods are limited by the voltage ripple of the x-ray tube and the low numbers of photons near the kVp energy. Common techniques for minimizing the polychromatic contamination in XRF setups include having the foil illuminated by an x-ray beam that is not directed towards the detector, and/or by placing a lead shield containing a pin hole between the detector and the foil [12, 13].

The proposed technique provides a powerful calibration tool measuring XRF with minimal polychromatic contamination using the native MARS scanner geometry. In addition, as the metallic foils can be permanently mounted inside the MARS scanner, it provides a highly automatable method for generating monochromatic photons that can then be used for energy calibration. This paper presents three aspects of our work towards developing this methodology. First, the experimental setup that we use to generate and measure oblique XRF is described. Second, we present a model for calculating the expected number of measurable XRF photons in this experimental setup. This enables optimization of experimental parameters to maximize XRF yield, particularly in more complex setups with multiple foils. Thirdly, we show some of our preliminary results of oblique XRF from molybdenum and lead foils with this setup.

2 Experimental setup

The MARS small bore scanner has a movable extrinsic filtration module that is located between the x-ray source and source collimators. This module enables different types of source filtration to be selected and used. In our setup we have placed several different metallic foils on the front of the 1 mm Al filter bar in this filtration module. These foils each produce XRF at different energies within our desired imaging range of 10–120 keV (shown in table 1). Examples of foil materials that we have chosen for our prototype setups include molybdenum, lead, tantalum, indium, neodymium, and dysprosium. When the "foil" filter bar is illuminated by the x-ray source each foil will generate XRF - assuming photons of sufficient energy are present in the incident x-ray beam for the given foil (i.e. the K-edge energy). The source collimators can then be used to isolate the XRF produced by a single foil from that of any other foil (figure 1). This also reduces the size of the main x-ray beam at the detector plane. The MARS camera can then be moved vertically into a position that is both outside of the main beam and where there is a sufficient XRF.

3 Oblique fluorescence model

This section describes the model that we have developed to calculate the oblique XRF production from the experimental setup described above. This description is broken into two parts. Firstly, the equation for the XRF produced by a narrow x-ray beam passing through a foil is given. Secondly, we describe how we adapt this equation to calculate the XRF generation from an illuminated foil. This section is concluded with an example of molybdenum fluorescence production predicted by this model.

2016 JINST 11 C12063

Table 1. K_α fluorescence and K-edge absorption energies for selected foil materials used in our prototype setups [14, 15]. These elements were chosen to provide a spread of XRF energies spanning our desired imaging range. The K-edge energy indicates the minimum incident photon energy required to produce K_α XRF from the given element.

Element	Mo	In	Nd	Dy	Ta	Pb
K-edge Energy (keV)	20.0	27.9	43.6	53.8	67.4	88.0
$K_{\alpha 1}$ Energy (keV)	17.5	24.2	37.4	46.0	57.5	75.0
$K_{\alpha 2}$ Energy (keV)	17.4	24.0	36.8	45.2	56.3	72.8

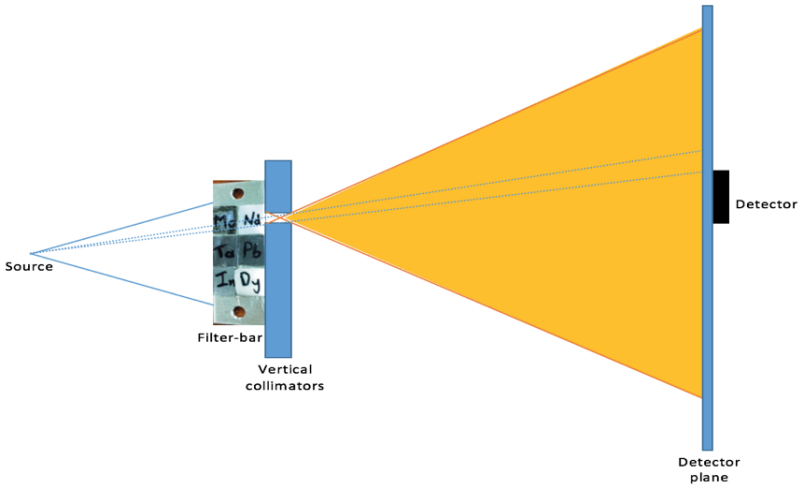

Figure 1. Illustrative diagram of experimental setup for measuring oblique XRF from metallic foils placed between the x-ray source and the source collimators. The collimators can be positioned to isolate XRF (yellow) from a specific foil outside of the main x-ray beam.

3.1 Narrow beam foil illumination

There are several factors to consider when describing the production of XRF from a narrow beam of x-rays passing through a foil. For this we only consider the production of K_α fluorescence photons. The production of other XRF photons such as K_β can be determined using an equivalent formulation. Firstly, the K_α photons are generated from the interactions of attenuated photons. However, not all attenuated x-rays produce K_α photons. The probability that an interaction results in K_α generation is given by the fluorescence yield, which depends on the foil material. In addition, after K_α photons are generated they themselves are potentially attenuated before they exit the foil. Taking these two processes into account, the number of K_α fluorescence photons escaping a foil of thickness L for an arbitrary input x-ray beam is given by:

$$N_{K_\alpha}(L) = \int_K^\infty \omega_{K_\alpha} I_0(E) \frac{\tau_{K_\alpha}(E)}{\mu_{K_\alpha} - \mu(E)} [e^{-\mu(E)L} - e^{-\mu_{K_\alpha} L}] dE \tag{3.1}$$

where ω_{K_α} is the fluorescence yield, $I_0(E)$ is the number of x-rays of energy E in the input beam, $\tau_{K_\alpha}(E)$ is the K_α photoelectric absorption contribution to the linear attenuation coefficient, μ_{K_α} is the linear attenuation of the foil at the energy of the K_α photons, and $\mu(E)$ is the linear attenuation of the foil for photons of energy E. The integration limits are defined for all x-rays in the incident

2016 JINST 11 C12063

x-ray beam with energies higher than the K-edge energy of the foil material. An approximation made in the derivation of this equation is that the thickness of the foil is infinitesimally small. To use this equation for thick foils, the fluorescence production would need to be calculated for different layers within the foil. This would enable the additional attenuation of the wide angle K_α photons produced in each layer of the foil to be accounted for. Further details on this derivation can be found in [16].

3.2 Complete foil illumination

When the entire foil is illuminated, each point on the foil can be treated as an independent XRF point source (figure 2). To determine the total XRF reaching different regions of the detector plane, contributions from all of these point sources must be combined. The contribution from a single point source is given by eq. (3.1), where the thickness of the foil L is replaced by the effective path length of the incident x-ray beam through the foil (figure 2). The XRF flux (in $photons/\mu sr$) from each point source on the foil is determined by dividing the number of respectively produced XRF photons by 4π. Combining the contributions of each point source at the detector plane requires the position of the collimators to be taken into account. Any XRF ray from any foil point source that is blocked from reaching the detector plane by the collimators (assumed to be ideal) need to be excluded from this cumulative sum.

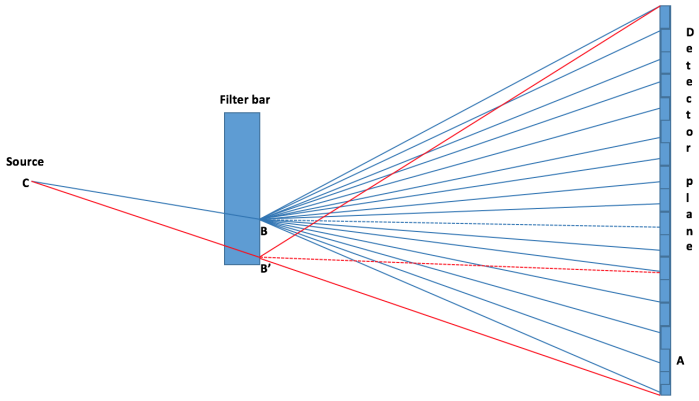

Figure 2. Two illuminated regions on the foil **B** and **B'** acting as independent point sources. Each point produces a different XRF flux, and the distances to the same points on the detector plane are mostly different.

3.3 Molybdenum foil example

An example of the predicted number of molybdenum XRF photons reaching different positions of the detector plane using this model is given in figure 3. Parameters used for this example were chosen to be similar to those used in our preliminary experimental work: an x-ray tube voltage of 40 kVp, a tube current of 350 μA, an exposure time of 10, 000 ms, a foil thickness of 50 μm, and a source-to-detector distance of 150 mm. The foil was divided into 128 point sources. The vertical center of detector plane was divided into 110 μm^2 tiles to match the our detector pixel size.

2016 JINST 11 C12063

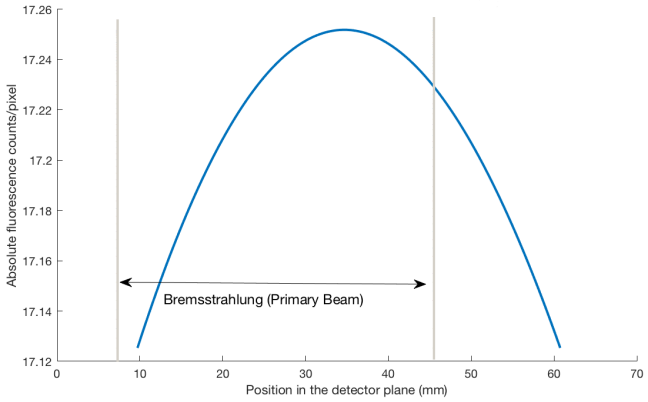

Figure 3. Expected number of molybdenum XRF photons across the vertical center of the detector plane for given model parameters.

4 Preliminary experiments

4.1 Methods

This section presents two preliminary experimental results we have obtained for measuring oblique XRF of molybdenum and lead foils with a CdTe-Medipix3RX detector. For a reference, the average energy response of the detector was determined beforehand using the kVp method for global energy calibration [11]. In each experiment, the positions of the collimators and detector were calculated to give minimal fluorescence contribution from the other foils attached to the filter bar as shown in figure 4. The measurement of molybdenum XRF used an x-ray tube voltage and anode current of 40 kVp and 350 μA respectively. The measurement of lead fluorescence used 95 kVp and 300 μA respectively. Both experiments used an exposure time of 10, 000 ms and had a source to detector distance of 150 mm. Measurements were then made at every threshold DAC. For each sampled DAC step, 50 frames was collected for molybdenum and 100 frames was collected for lead. The frames were then averaged for each sampled DAC, and then subtracted to obtain differential spectra. To avoid negative counts due to the quantum noise, we preferred to do the subtraction between every third threshold DAC.

4.2 Results

Figure 5 shows the differential spectra measured by the first charge summing mode counter for one pixel in the detector. Each spectra shows a well defined peak in the expected regions for their respective fluorescence photon energies. These peaks are at a DAC value of 54 for Mo and 177 for Pb. Similar trends were observed in other detector pixels. The global energy calibration map for this counter was $Th = 2.08\,E + 19.2$ where Th is the threshold DAC value and E is the threshold energy in keV. Using the global energy calibration map to convert peak DAC values to photon energy, we obtain energies of 16.3 keV for molybdenum and 75.9 keV for lead. Comparing these global map energies to the $K_{\alpha 1}$ fluorescence energies in table 1, it is observed that for this pixel (for the given counter) the energy response of at a DAC value of 54 is offset by -1.2 keV from the global calibration estimate, and the DAC value of 177 is offset by 0.9 keV. These energy offset values fall

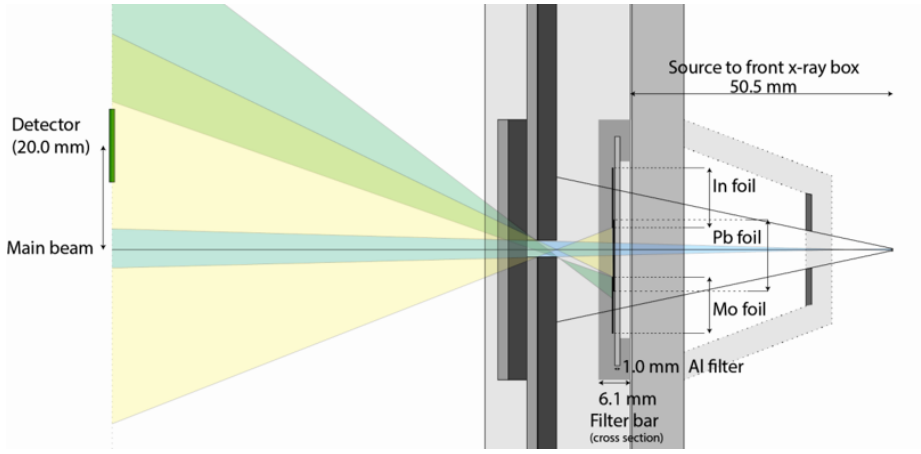

Figure 4. Setup for identifying isolated region of lead XRF at the detector plane. The vertical and horizontal collimators are positioned to block fluorescence generated by the other foils attached to the filter bar. The desired region of isolated lead XRF (yellow) sits between the main x-ray beam and wide angle XRF generated from the other foils (green).

within the range expected by previous measurements we have made on the dispersion of the the detector's pixel energy response [11].

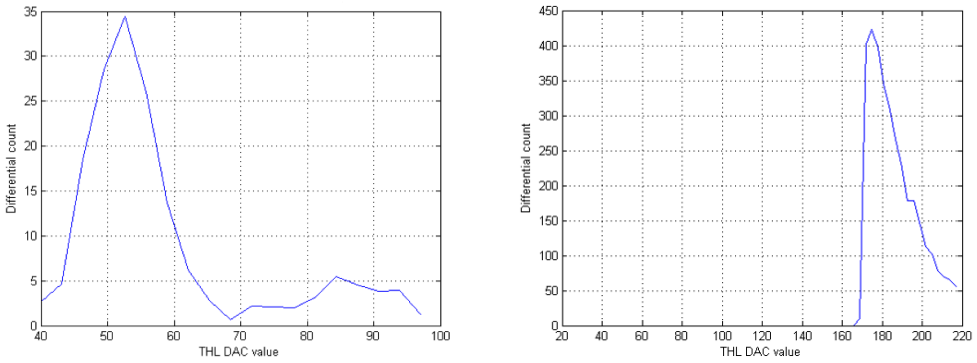

(a) **(b)**

Figure 5. Measured XRF distributions produced from (a) molybdenum, and (b) lead foils for a single detector pixel. Each measurement shows a well defined peak in the region expected for the given fluorescence energy. Similar trends were observed for other well behaved pixels.

5 Discussion

Our preliminary experimental results of the presented methodology indicate that we can observe oblique XRF from molybdenum and lead metallic foils with minimal bremstrahlung contamination from the main x-ray beam. The experimental result for molybdenum was approximately a factor of 10 greater than the corresponding modeled XRF distribution with similar setup parameters. There are several possible reasons for this. There may be discrepancies in the parameters between the model and experiment that have not been accounted for. For example, a 1–2 μm variation in

2016 JINST 11 C12063

the thickness of a 50 μm molybdenum foil could result in a significant discrepancy in the number of XRF photons escaping the foil [16]. It is also possible that the focal spot inside the x-ray tube in our setup is closer to the front of the tube than we expected. This would also result in a larger experimental result as we have observed. The modeled XRF distribution example only represents the K_α photon contribution, whereas in addition there will also be K_β fluorescence present in the measurement. The experimental setup in the presented method is used to measure transmission fluorescence. Measurements from such setups suffer from more Compton scattering contamination than typical reflection setups. However as shown by Butler et al., it is possible to construct transmission type setups which produce strong fluorescence signals despite the increase in scatter [17]. In other transmission setups such as in Tran et al. the Compton scatter contribution is deemed to be negligible [18]. The narrow collimation in our setup should give rise to increased scatter in the field of view [17]. This is also indicated in some of our observations during our experimental work. Despite this, we have shown that a reasonable fluorescence signal is detectable in the given setup. We are in the process of investigating these potential effects and refining this methodology further. In addition, we are looking towards repeating our experimental measurements with a wider range of metallic foils, and using a variety of detectors with different sensor layers (including CdTe, CZT, GaAs, and Si). We have also done preliminary work investigating the optimal thickness of the metallic foils in our setup to improve the XRF yield from this methodology, which we intend to incorporate into future experiments.

6 Conclusion

We have presented a methodology for generating XRF from metallic foils in a MARS spectral CT scanner that can be measured with minimal contamination from the main polychromatic x-ray beam. This is done by placing the metallic foils behind the source collimators, enabling oblique angle fluorescence to reach areas of the detector plane outside of the main x-ray beam. Our preliminary experimental results shows that we are capable of measuring this oblique XRF signal. Through comparisons with the detector's global energy calibration, the observed peaks were shown to be within the expected dispersion of the pixel energy response. We have also presented a model for predicting the oblique XRF distribution at the detector plane. This model assists in determining the position of optimal isolated XRF yield, particularly in multi-foil setups. We are currently working towards refining this methodology; investigating potential sources of discrepancies between our model and experimental results; and expand our experimental analysis to consider a wider variety of metallic foils and detector sensor layers.

References

[1] R.E. Alvarez and A. Macovski, *Energy-selective reconstructions in x-ray computerised tomography*, *Phys. Med. Biol.* **21** (1976) 733.

[2] H.Q. Le and S. Molloi, *Segmentation and quantification of materials with energy discriminating computed tomography: A phantom study*, *Med. Phys.* **38** (2011) 228.

[3] K. Taguchi et al., *Modeling the performance of a photon counting x-ray detector for ct: Energy response and pulse pileup effects*, *Med. Phys.* **38** (2011) 1089.

2016 JINST 11 C12063

[4] S. Kappler, D. Niederlöhner, K. Stierstorfer and T. Flohr, *Contrast-enhancement, image noise, and dual-energy simulations for quantum-counting clinical CT*, *Proc. SPIE* **7622** (2010) 76223H.

[5] B.J. Heismann, B.T. Schmidt and T. Flohr, *Spectral computed tomography*, SPIE (2012).

[6] R. Ballabriga et al., *The Medipix3RX: A high resolution, zero dead-time pixel detector readout chip allowing spectroscopic imaging*, 2013 *JINST* **8** C02016.

[7] R. Ballabriga, M. Campbell, E. Heijne, X. Llopart, L. Tlustos and W. Wong, *Medipix3: A 64k pixel detector readout chip working in single photon counting mode with improved spectrometric performance*, *Nucl. Instrum. Meth.* **A 633** (2011) S15.

[8] J. Ronaldson et al., *Characterization of Medipix3 with the MARS readout and software*, 2011 *JINST* **6** C01056.

[9] E. Gimenez et al., *Study of charge-sharing in MEDIPIX3 using a micro-focused synchrotron beam*, 2011 *JINST* **6** C01031.

[10] T. König, *Exploring coherent phenomena and energy discrimination in x-ray imaging*, http://www.ub.uni-heidelberg.de/archiv/11933 (2011).

[11] R.K. Panta et al., *Energy calibration of the pixels of spectral x-ray detectors*, *IEEE Trans. Med. Imag.* **34** (2015) 697.

[12] J. Uher, G. Harvey and J. Jakubek, *X-ray fluorescence imaging with the medipix2 single-photon counting detector*, *IEEE Trans. Nucl. Sci.* **59** (2012) 54.

[13] P. Bruyndonckx, A. Sasov and X. Liu, *Laboratory 3d micro-xrf/micro-ct imaging system*,*AIP Conf. Proc.* **1365** (2010) 61.

[14] J. Hubbell and S. Seltzer, *Tables of x-ray mass attenuation coefficients and mass energy-absorption coefficients (version 1.4)*, http://physics.nist.gov/xaamdi [Accessed: 27 September 2016], (2004).

[15] R. Deslattes et al., *X-ray transition energies (version 1.2)*, http://physics.nist.gov/XrayTrans [Accessed: 27 September 2016], (2005).

[16] L. Vanden Broeke, *Foil fluorescence in mars spectral imaging*, MSc Thesis, University of Canterbury, U.K. (2015).

[17] A. Butler et al., *Measurement of the energy resolution and calibration of hybrid pixel detectors with GaAs:Cr sensor and Timepix readout chip*, *Phys. Part. Nucl. Lett.* **12** (2015) 59 [arXiv:1501.03334].

[18] C. Tran, M. De Jonge, Z. Barnea and C. Chantler, *Absolute determination of the effect of scattering and fluorescence on x-ray attenuation measurements*, *J. Phys.* **B 37** (2004) 3163.

2016 JINST 11 C12063